INTERNATIONAL JOURNAL FOR NUMERICAL METHODS IN FLUIDS, VOL. 9, 1331–1352 (1989)

TWO-DIMENSIONAL SUBCRITICAL AND SUPERCRITICAL OPEN CHANNEL FLOW CALCULATION USING A TIME-MARCHING METHOD

JOHANNES VASSILIOU SOULIS

Civil Engineering Department, Demokrition University of Thrace, Xanthi, Greece

SUMMARY

A time-marching method is presented for the calculation of two-dimensional, high-speed channel flow, including the usually neglected terms of slope and bottom friction. Time-marching methods are potentially the most flexible means of calculating flow through geometrically complex channel passages, since they can readily deal with subcritical and supercritical flows. The adopted numerical scheme comes straight from gas flow computations in turbomachines. The flow is assumed to be fully mixed in the vertical direction, so that vertical variations may be neglected. Comparisons with other numerical solutions for various open channel configurations show that the proposed approach is a comparatively accurate, reliable and fast technique. It can be utilized for open channel designs.

KEY WORDS Finite volume Time-marching High-speed free-surface flow

INTRODUCTION

In recent years significant advances have been made in computational fluid dynamics applied to open channels. Many approaches have been taken to the general problem of open channel flow calculation. Thus mathematical models exist at various levels of sophistication. Obviously the detailed description of flow phenomena is best accomplished in a three-dimensional environment. However, the complexity of a formulation in three dimensions requires tremendous amounts of computational effort. By assuming that the flow is fully mixed in the vertical direction, a two-dimensional analysis may be employed. A further assumption of hydrostatic pressure distribution seems to be valid if the water surface is not too rough and it is the objective of the designer to create a smooth water surface. Also, if zero slope and zero friction are assumed, the governing flow equations become simple enough to permit numerical solution. Such solutions have been presented by Ippen,[1] Rouse *et al.*[2] and others. Busemann's[3] method of characteristics was applied by Ippen and Dawson[4] to calculate the hydraulic jumps produced in supercritical flow in channels with varying cross-sectional area. Liggett and Vasudev[5] have presented a numerical solution for 2D high-speed channel flow including slope and friction effects. Charts were presented which gave an indication of the magnitude of the departure of the improved solution from the frictionless zero-slope solutions. Two-dimensional finite difference calculation methods have been developed by McGuirk and Rodi[6] which describe the circulation region immediately downstream of a side discharge into a flowing river. Chapman and Kuo[7,8] have applied a finite difference technique to the solution of the depth-integrated equations of motion in a wide shallow rectangular channel

0271–2091/89/111331–22$11.00

Received March 1988
Revised December 1988

with and without an abrupt expansion. Demuren[9,10] presented a two-dimensional numerical procedure, based on the GENMIX code of Spalding,[11] for calculating both supercritical and subcritical flows in open channels with varying cross-section. Predictions agreed well with experimental data over a wide range of cases so long as three-dimensional effects did not become very important. Villegas[12] used the method of three characteristics derived by Vasudev[13] to calculate the flow for the Punchina dam spillway in Columbia. From the analysis he concluded that it is possible to use the theory of two-dimensional open channel flow for the design of spillways of varying depth. The program ran smoothly for most of the converging part of the spillway, but several problems developed upstream of the constant width zone of the channel. This constant width zone was located in the downstream region of the converging spillway. The approach of Herbich and Walsh[14] is based on the method of two characteristics assuming inclined frictionless two-dimensional flow with hydrostatic pressure distribution.

The analogy between free surface water flows and compressible gas flows was pointed out by, among others, Riabouchinsky.[15] Time-marching solutions of the Euler equations are now widely used for the analysis of flow through turbomachine blade rows.[16-18] Their main attraction is the ability to compute mixed subsonic–supersonic flows with automatic capturing of shock waves. A computer program based on Denton's[17] time-marching is employed in all current research calculations. Thus a two-dimensional high-speed channel flow calculation including the usually neglected terms of slope and bottom friction is presented. The time-marching method is more flexible than others because of its ability to handle subcritical and supercritical types of flow. Other very important features of the method are its great simplicity and the physical understanding obtained from the solution procedure. On the contrary, a finite difference approach requires a co-ordinate transformation, which is quite complicated for varying cross-section channels, whereas the use of the finite element method involves a rather complex and heavy mathematical formulation.

The method has been applied to a simple straight wall channel configuration to compute the water surface profiles and comparisons have been made with numerical solutions. In addition, some calculations have been performed on a gradually expanding open channel flow configuration. Some slope and friction effects are presented which give an indication of the magnitude of the departure from the frictionless zero-slope solution.

The results presented here are a first step towards a test application with a turbulence closure model to solve the depth-integrated equations of motion for steady free surface flows. Near future extensions of the current research work will include hydraulic jump computations. The addition of the energy equation is sufficient to define the solution of mixed continuous–discontinuous flows. This is a straightforward procedure and requires minimum computational programming effort.

FLOW EQUATIONS

The channel flow will be assumed to be homogeneous, incompressible, two-dimensional and viscous with wind and Coriolis forces neglected. A hydrostatic pressure distribution is assumed throughout the flow field. Thus the governing flow equations for the physical domain, where the Cartesian co-ordinate system is introduced, are

$$-\frac{\partial h}{\partial t}=\frac{\partial (hu)}{\partial x}+\frac{\partial (hv)}{\partial y} \qquad \text{(continuity)}, \tag{1}$$

$$-\frac{\partial (hu)}{\partial t}=\frac{\partial (gh^2/2+hu^2)}{\partial x}+\frac{\partial (huv)}{\partial y}-gh(S_{0x}-S_{fx}) \qquad (x\text{-momentum}), \tag{2}$$

$$-\frac{\partial(hv)}{\partial t}=\frac{\partial(huv)}{\partial x}+\frac{\partial(gh^2/2+hv^2)}{\partial y}-gh(S_{0y}-S_{fy}) \quad (y\text{-momentum}). \tag{3}$$

Here x and y represent the Cartesian co-ordinate positions in the longitudinal and transverse directions respectively; t is the time; u and v are the averaged velocity components in the x- and y-directions respectively; h is the water depth; g is the accelaration due to gravity; $S_{0x}(=-\partial z_0/\partial x)$ and $S_{0y}(=-\partial z_0/\partial y)$, where z_0 is the bottom elevation, are channel slopes in the x- and y-directions respectively; and S_{fx} and S_{fy} are the friction slopes in the x- and y-directions respectively. The friction slopes are defined as

$$S_{fx}=\frac{u\sqrt{(u^2+v^2)}}{hC^2}, \tag{4}$$

$$S_{fy}=\frac{v\sqrt{(u^2+v^2)}}{hC^2}, \tag{5}$$

where C is Chézy's friction coefficient for flow. Another option calculates the friction slopes using Manning's friction coefficient n. By writing the equation for frictional resistance in this way, it was assumed that all of the resistance is due to bottom friction, thus neglecting the boundary layer on the side walls. The depth-integrated effective stress has been neglected in order to eliminate the possibility of introducing numerical smoothing.

COMPUTATIONAL GRID

The finite volume (cell) elements used for the current numerical scheme are formed by quasi-streamlines and transverse lines, where the element nodes are located at each of the four corners (Figure 1).

In practice, a grid such as that shown in Figure 2 is used for channel flow calculations. The numerical scheme allows complete flexibility in choosing the spacing in both streamwise and transverse directions. This type of grid is the most common choice in channel flow calculations.

However, its use imposes severe limitations on accuracy when the elements become highly skewed. Numerical errors are likely to occur in the very changes in flow around a highly concave (convex) area of the channel and these will then influence the flow on the whole side of the channel. Hence it is essential that sufficient grid points are located around the highly curved sides of the channel. The use of transverse lines greatly facilitates application of the periodicity condition

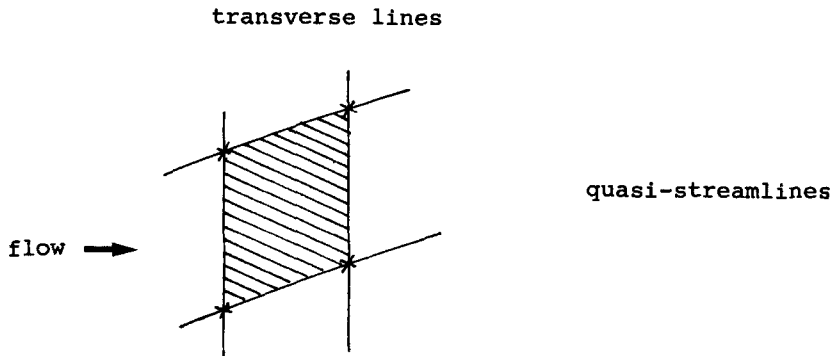

Figure 1. Typical finite volume (cell) used for time-marching calculation

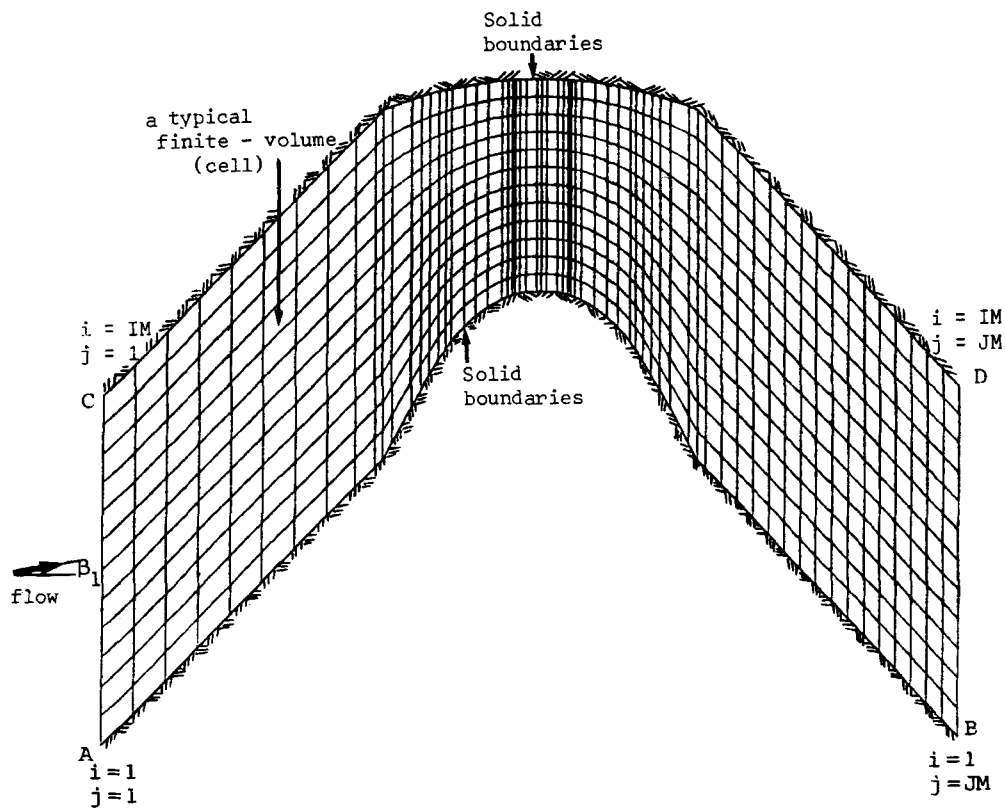

Figure 2. Computational mesh used for open channel flow time-marching calculation

between the limiting quasi-streamlines upstream of the flow passage. Periodic boundaries may arise in cases where the flow passes through geometrically symmetric obstacles, e.g. between the piers of a bridge. The direction of these limiting streamlines need not coincide with the inlet flow direction.

NUMERICAL FORMULATION

A major improvement[16] was obtained by solving the equations of flow (1)–(3) in integral form, i.e. by applying the equations of continuity, x-momentum and y-momentum to a series of finite volumes with adjacent volumes sharing a common face. In this way, once the steady state is reached, the net flux into each elemental volume is zero, so that overall mass is conserved and changes of momentum equate to the forces imposed by the boundaries of the system under consideration. The two-dimensional flow equations may be written as conservation equations for a control volume ΔV of unit height and for a time step Δt as

$$-\Delta h = [\Delta(hu)\Delta y + \Delta(hv)\Delta x]\frac{\Delta t}{\Delta x \Delta y}, \tag{6}$$

$$-\Delta(hu) = \left[\Delta\left(\frac{gh^2}{2} + hu^2\right)\Delta y + \Delta(huv)\Delta x\right]\frac{\Delta t}{\Delta x \Delta y} - gh(S_{0x} - S_{fx})\Delta t, \tag{7}$$

$$-\Delta(hv) = \left[\Delta(huv)\Delta y + \Delta\left(\frac{gh^2}{2} + hv^2\right)\Delta x\right]\frac{\Delta t}{\Delta x \Delta y} - gh(S_{0y} - S_{fy})\Delta t. \tag{8}$$

Figure 3 shows the notation used for mass flux balancing across a finite volume (cell) of the flow. Similar notation is adopted for the balancing of the x-momentum and y-momentum fluxes. Thus,

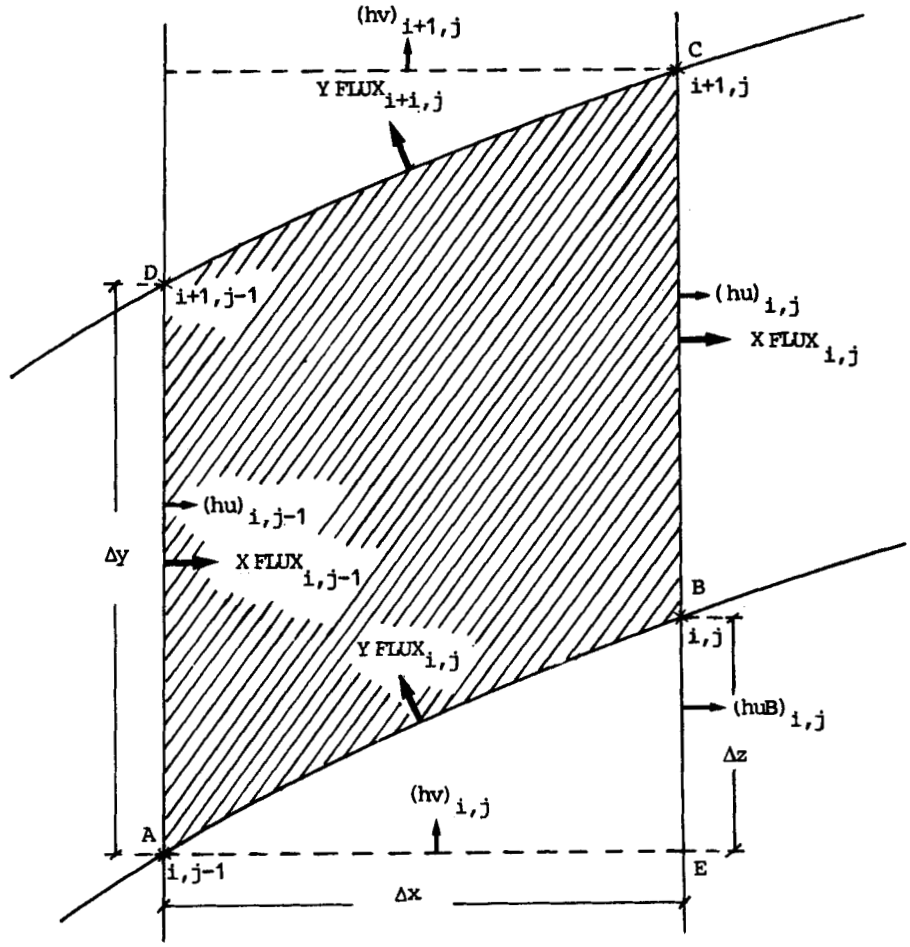

$$\text{XFLUX}_{i,j} = (hu)_{i,j}\,\Delta y$$

$$\text{YFLUX}_{i,j} = (hv)_{i,j}\,\Delta x - \Delta z\,(huB)_{i,j}$$

where

$$(huB)_{i,j} = \frac{(hu)_{i,j} + (hu)_{i,j-1}}{2}$$

$$(hu)_{i,j} \equiv \frac{(hu)_{i+1,j} + (hu)_{i,j}}{2}$$

$$(hv)_{i,j} \equiv \frac{(hv)_{i,j} + (hv)_{i,j-1}}{2}$$

Figure 3. Notation for the mass flux across a finite volume (cell)

for the mass flux, an XFLUX at point i,j is defined as

$$(\text{XFLUX})_{i,j}=\left[\frac{(hu)_{i,j}+(hu)_{i+1,j}}{2}\right]\Delta y, \tag{9}$$

while the YFLUX, at the same point i,j is defined as

$$(\text{YFLUX})_{i,j}=\left[\frac{(hv)_{i,j}+(hv)_{i,j-1}}{2}\right]\Delta x-\left[\frac{(hu)_{i,j}+(hu)_{i,j-1}}{2}\right]\Delta z. \tag{10}$$

The second term of the RHS of the above equation comes from the balancing of the mass fluxes into the ABE flow region. The Δz term is defined in Figure 3.

For the x-momentum flux balance, the corresponding $(\text{XFLUX})_{i,j}$ and $(\text{YFLUX})_{i,j}$ are defined as

$$(\text{XFLUX})_{i,j}=\left[\frac{(gh^2/2+hu^2)_{i,j}+(gh^2/2+hu^2)_{i+1,j}}{2}\right]\Delta y, \tag{11}$$

$$(\text{YFLUX})_{i,j}=\left[\frac{(huv)_{i,j}+(huv)_{i,j-1}}{2}\right]\Delta x-\left[\frac{(gh^2/2+hu^2)_{i,j}+(gh^2/2+hu^2)_{i,j-1}}{2}\right]\Delta z. \tag{12}$$

For the y-momentum flux balance, the corresponding $(\text{XFLUX})_{i,j}$ and $(\text{YFLUX})_{i,j}$ are defined as

$$(\text{XFLUX})_{i,j}=\left[\frac{(huv)_{i,j}+(huv)_{i+1,j}}{2}\right]\Delta y, \tag{13}$$

$$(\text{YFLUX})_{i,j}=\left[\frac{(gh^2/2+hv^2)_{i,j}+(gh^2/2+hv^2)_{i,j-1}}{2}\right]\Delta x-\left[\frac{(huv)_{i,j}+(huv)_{i,j-1}}{2}\right]\Delta z. \tag{14}$$

The terms $\Delta(hu)$ and $\Delta(hv)$ in equation (6) are defined as

$$\Delta(hu)=(\text{XFLUX})_{i,j}-(\text{XFLUX})_{i,j-1}, \tag{15}$$

$$\Delta(hv)=(\text{YFLUX})_{i+1,j}-(\text{YFLUX})_{i,j}. \tag{16}$$

Similar differencing is adopted for the terms $\Delta(gh^2/2+hu^2)$, $\Delta(gh^2/2+hv^2)$ and $\Delta(huv)$ of equations (7) and (8). The slopes S_{0x} and S_{0y} are precalculated and stored, while the friction slopes S_{fx} and S_{fy} are updated in each time step. For all the above slopes, averaged values of the appropriate physical quantities are used.

All these fluxes may now be used in the RHS of equations (6), (7) and (8) to obtain the changes in h: (Δh), hu: $\Delta(hu)$ and hv:$\Delta(hv)$ respectively. A problem arises as to how these changes should be distributed between the four corners A, B, C and D of the finite volume (cell) of Figure 3. This distribution affects the stability and time dependence of the method but not the steady state solution. Once a steady state solution is obtained, the sum of the fluxes of each conserved variable over the faces of each finite volume will be zero, and hence the conservation equations satisfied, irrespective of how these changes were distributed.

In the current research work it was decided to send half of the information regarding the changes in water depth h as well as in hu and hv to the upstream face of the finite volume involved, while the other half is sent to the downstream corners. This scheme was found to be stable. The changes Δh, $\Delta(hu)$ and $\Delta(hv)$ were not used directly to yield the h, hu and hv values. For all test runs two different amplification factors were used: a C_1 factor for the h estimation and a C_2 factor for

the hu and hv estimations. The procedure is as follows:

$$h_{i,j}^{(n+1)} = h_{i,j}^{(n)} + \frac{\Delta h_{i,j}^{(n+1)}}{1 + |C_1 \Delta h_{i,j}^{(n+1)}|}, \tag{17}$$

where

$$C_1 = 10.0/h_{1,1}^{(0)}, \tag{18}$$

and

$$(hu)_{i,j}^{(n+1)} = (hu)_{i,j}^{(n)} + \frac{\Delta(hu)_{i,j}^{(n+1)}}{1 + |C_2 \Delta(hu)_{i,j}^{(n+1)}|}, \tag{19}$$

where

$$C_2 = 2.5/(hu)_{1,1}^{(0)}, \tag{20}$$

and similarly for the $(hv)^{(n+1)}$ estimation. The numerical scheme was found to be stable over the wide range of C_1 and C_2 values considered.

The appearence of the time derivative terms in the equations of motion (6)–(8) should not be misinterpreted as an attempt to address unsteady flow phenomena. Strictly speaking, the time-marching method may only be applied to steady flow problems, and consequently the first-order time integration employed is simply a convenient way to iterate to a steady state solution. Table I gives details of the iterative scheme. The order in which the x- and y-momentum equations are solved is not important. For the scheme to be effective, the equations must be solved in the order: continuity → momentum.

BOUNDARY CONDITIONS

At the upstream boundary AC of Figure 2 a relative flow direction is specified. At the downstream boundary BD a specified, uniform across the width, water depth is assumed. Across the channel a fixed value for the flow rate is also specified. All the above boundary conditions have been proved to be valid for subcritical flow entrance. In cases where a mixed subcritical–supercritical type of flow is encountered (always subcritical entrance), a value for the upstream total head is specified instead of the flow rate across the channel.

For supercritical flow entrance, at the upstream boundary AC the transverse flow direction component of velocity is specified along with a uniform across the width, water depth. A value for the total head is also specified for the upstream boundary AC.

In cases where periodic flow is to be calculated (not included in the current research work), the periodicity condition on the bounding streamwise lines upstream and downstream of the flow passage is easily satisfied by first treating points on these lines as interior points and then equating values at corresponding points on two boundaries.

When the condition of no mass flow across the solid boundaries is applied, the fluxes hu and hv are taken across the faces of the boundary finite volume, which is bounded on one face by the body surface (Figure 4). Thereafter, the hu and hv flux components for the solid boundaries are recalculated with the requirement that the component of velocity normal to the solid face be zero.

The inputs of the current research programme also include a longitudinal bottom slope, a transverse bottom slope of zero value and a friction coefficient.

NUMERICAL RESOLUTION

A numerical algorithm has been presented for solving the equations of two-dimensional high-speed channel flow. Iterations were continued until the average change of longitudinal flow

Table I. Outline of the iterative scheme

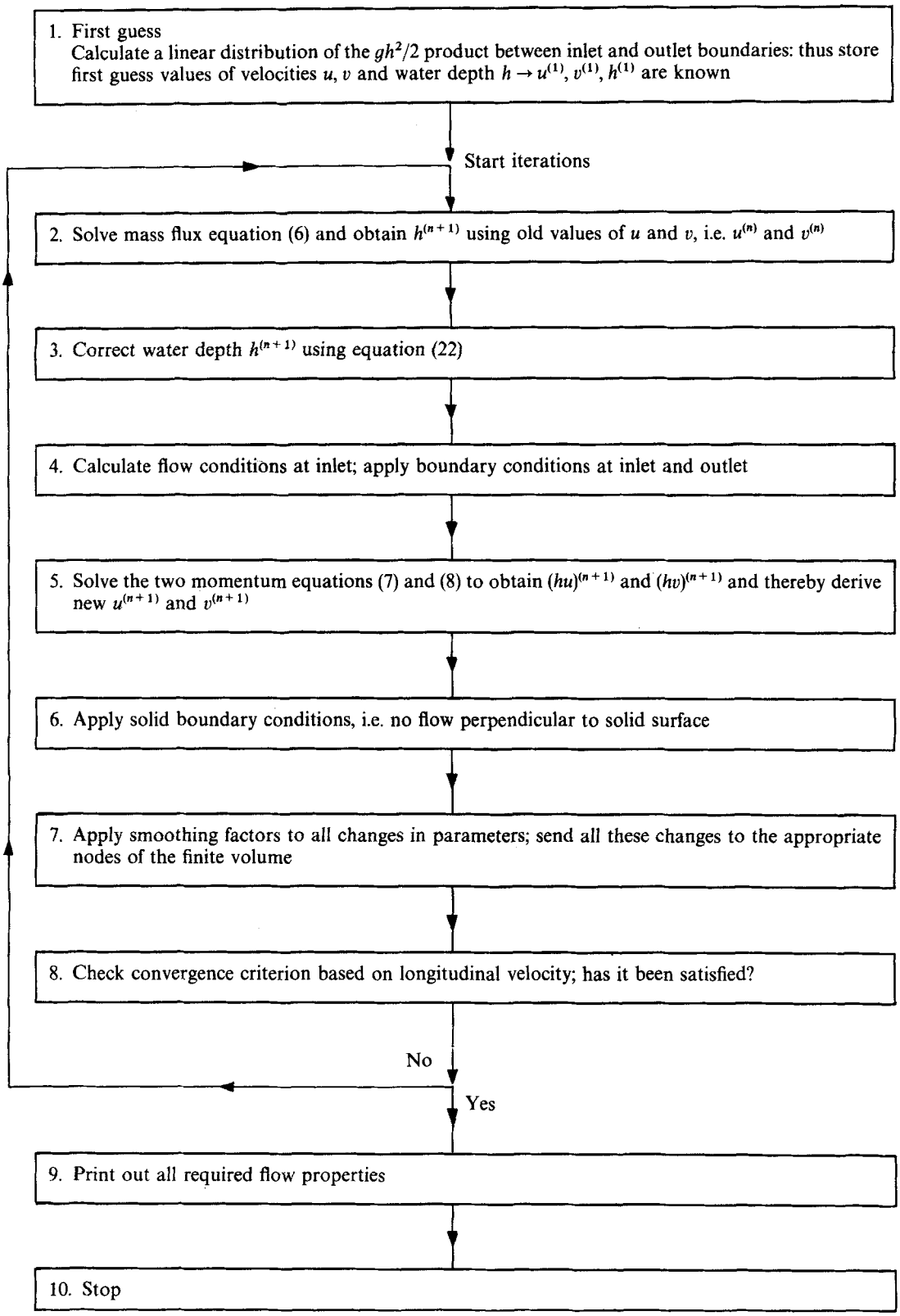

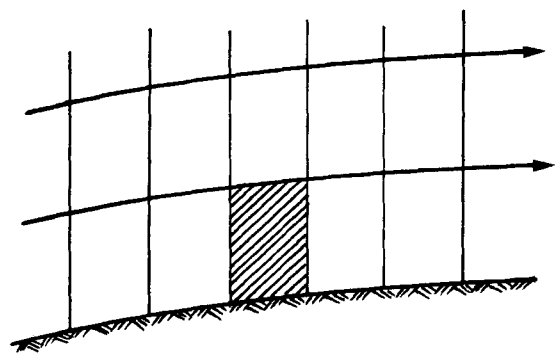

Figure 4. Solid boundary finite volume (cell) for the first computational row ($i = 1, j = 1$, JM)

velocity between successive iterations dropped below 0·001%. The run time per point per iteration was $1{\cdot}15 \times 10^{-2}$ s on a SPERRY-UNIVAC 90/30 computer. The total number of iterations required for convergence was about 2000, depending upon the geometry complexity and type of flow. The total CPU time for an 8×39 grid was about 6695 s on the above computer.

As with all time-marching methods, the theoretical maximum stable time step Δt is determined by the CFL criterion

$$\Delta t \leqslant \frac{\Delta x}{u + \sqrt{(gh)}}, \tag{21}$$

where Δx is the streamwise distance between the upstream and downstream faces of an element. Usually, instead of Δx, a $\Delta x_{\min}$ distance is used. The $\Delta x_{\min}$ distance is calculated as the minimum value of all Δxs of the grid used. Although different values of the physical time step, for each element could have been used, in the order to advance the convergence procedure for current research purposes a fixed value of Δt was chosen.

The integration of equations (6)–(8) through time, in order to reach a steady state solution, could have been performed using either an explicit or an implicit scheme. Implicit schemes involve some form of matrix inversion but allow larger time steps to be taken into consideration. Hence the steady state solution is reached in fewer but more costly time steps than with an explicit scheme. The current method is categorized as an explicit technique limited to the CFL criterion. The CFL essentially says that pressure waves cannot propagate by more than one grid spacing per time step. This means that if there are JM grid points in the longitudinal direction, the number of time steps required to reach a steady state from an arbitrary initial guess is of the order $50 \times$ JM. order. Thus many hundreds of time steps will be needed for convergence.

The most common source of inaccuracy arises at a blunt leading edge of the tested hydraulic structures where the relative coarse grid cannot resolve adequately the rapid changes in the flow properties. Then, a large number of grid points must be used to obtain an accurate solution around such structures.

During an iteration the water depth $h_{i,j}^{(n+1)}$ is corrected according to the formula

$$h_{i,j}^{(n+1)} = \omega \tilde{h}_{i,j}^{(n+1)} + (1-\omega) \tilde{h}_{i,j+1}^{(n+1)}, \tag{22}$$

where $\tilde{h}_{i,j}^{(n+1)}$ denotes the current, but not updated value, and ω is a correction factor. For nearly all applications it was decided that ω should take the value 0·5.

The terms $gh(S_{0x}-S_{fx})\Delta t$ and $gh(S_{0y}-S_{fy})\Delta t$ of equations (7) and (8) respectively were relaxed before they were incorporated into the flow equations. A typical relaxation factor for all test runs was 0·9.

A realistic guess for the expected water depth distribution is suggested. This will drastically reduce the amount of CPU time spent to achieve convergence. The program starts with an initial linear $gh^2/2$ distribution between the inlet and outlet flow regions of the hydraulic structure. Thereafter, an initial flow distribution is estimated using channel slopes and water depths.

APPLICATIONS

The first subcritical flow test is a straight parallel wall channel of rectangular cross-section as shown in Figure 5. The problem selected comprises a flow rate of 20·0 $m^3\ s^{-1}$ with an average exit depth h_2 of 2·0 m and an inlet flow angle β_1 of 0·0°. In order to get an indication of the time-marching computed results, it was decided to employ a standard, quasi-2D, fixed step numerical method. The water depth profiles are computed in the form

$$h_{i+1} = h_i + (S_0 - S_f)(x_{i+1} - x_i) - \frac{u_{i+1}^2}{2g} + \frac{u_i^2}{2g}. \tag{23}$$

A definition sketch is shown in Figure 6. In performing the numerical integration, the $\Delta x = (x_{i+1} - x_i)$ step is held constant, S_f is evaluated using Chézy's equation, h_{i+1} = constant at $x_{i+1} = 0{\cdot}0$, S_0 is constant and Q is also constant. This technique enables variable width channel flows to be calculated.

A comparison between time-marching and the above described standard fixed step method predictions of velocity and water depth distributions with $C = 50{\cdot}0$ (Chézy's friction coefficient) at $S_{0x} = 0{\cdot}01$ and $S_{0x} = 0{\cdot}02$ is shown in Figure 7. Actually, this figure shows the variation of centreline velocities and water depths as compared to the frictionless zero-slope solution, which is denoted by the subscript 'ir' (irrotational). The agreement between the two numerical methods is satisfactory. It must be emphasized that the velocity throughout the flow field is subcritical ($Fr = u/\sqrt{(gh)} < 1{\cdot}0$). A comparison between time-marching and the fixed step method predictions of velocity and depth distributions for the above channel at $Q = 20{\cdot}0\ m^3\ s^{-1}$, $h_2 = 2{\cdot}0$ m, $S_{0x} = 0{\cdot}01$ and $\beta_1 = 0{\cdot}0°$ using various Chézy friction coefficients, ranging between $C = 20.0$ and frictionless flow, is shown in Figure 8. The agreement is again satisfactory.

The channel transition shown in Figure 9 was used to test the numerical solution for supercritical flow. The length of the expansion is $11b$, where b is the half entrance width, and the final width is $1{\cdot}5b$. The expansion was tested for an entrance Froude number of 2·0 and a width ratio h/b at entrance of 0·5. For all numerical calculations the expansion produces reasonably

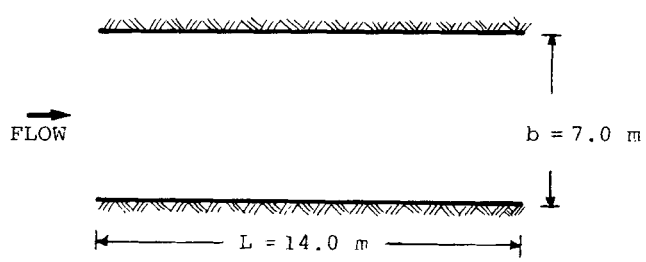

Figure 5. Straight parallel wall channel geometry

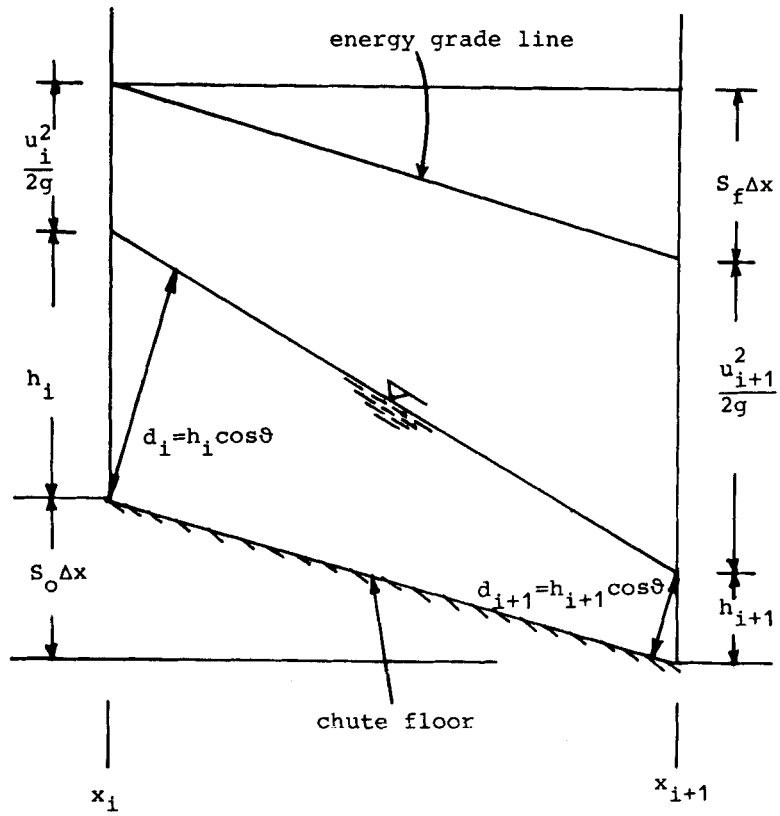

Figure 6. Definition sketch for gradually varied flow

smooth water surfaces. Figures 10(a), (b) and (c) show the variation of the centreline velocities in the improved solution as compared to the frictionless zero-slope solution for steep, mild and flat slopes respectively. The actual flow conditions at entrance were: total head $H_{01} = 5{\cdot}25$ m, water depth $h_1 = 1{\cdot}75$ m, transverse velocity $v_1 = 0{\cdot}0$ m s^{-1}. As expected, the slope and friction have a cancelling effect.

Figures 11, 12 and 13, 14 show the average exit velocity and water depth respectively as functions of slope and friction. The maximum effects of slope and friction are of the order of 20% over the ranges considered.

The third flow test is a divergent channel geometry of rectangular cross-section. The channel geometry is shown in Figure 9 with $b = 1{\cdot}75$ m and a total expansion length L of 15·0 m. The subcritical flow problem selected uses a flow rate of 5·0 m^3 s^{-1}, an average exit flow depth h_2 of 2·0 m, an inlet flow angle β_1 of 0·0°, a bottom slope of 0·0 and zero friction. A comparison between time-marching and the fixed step method predictions of velocity and depth distributions for the linearly expanding channel geometry is shown in Figure 15. Total velocity and depth values averaged across the channel width are used for the time-marching predicted results. The agreement is reasonably good.

The channel expansion shown in Figure 16 was used: (a) to test the accuracy of the time-marching solution by comparing it with a characteristics method; and (b) to get an indication of the magnitude of the departure from the frictionless zero-slope solution. This expansion was

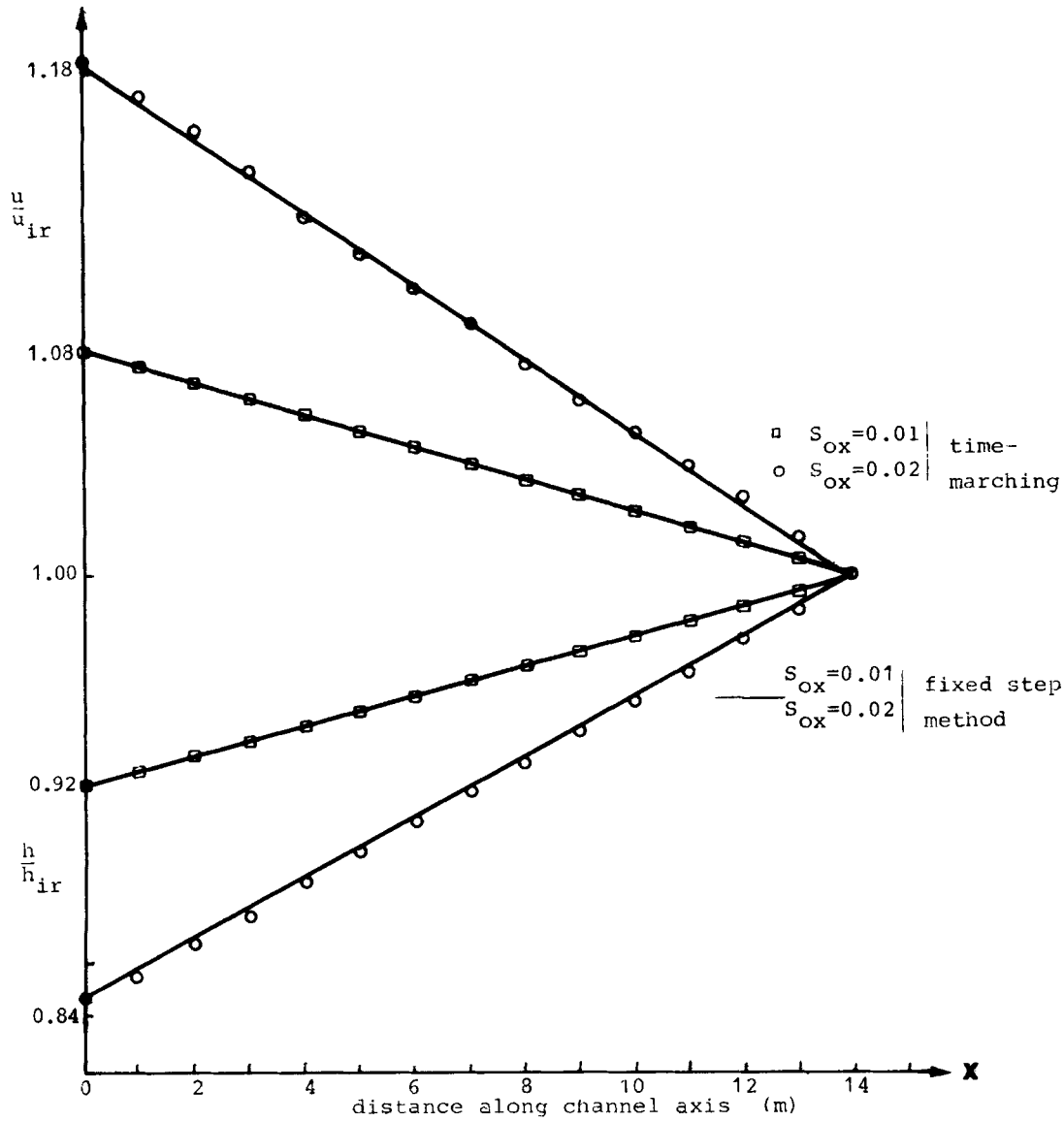

Figure 7. Comparison between time-marching and fixed step method predictions of subcritical velocity and depth distributions for straight parallel wall channel geometry at $Q = 20{\cdot}0\ m^3\ s^{-1}$, $h_2 = 2{\cdot}0$ m and $C = 50{\cdot}0$ using various slopes

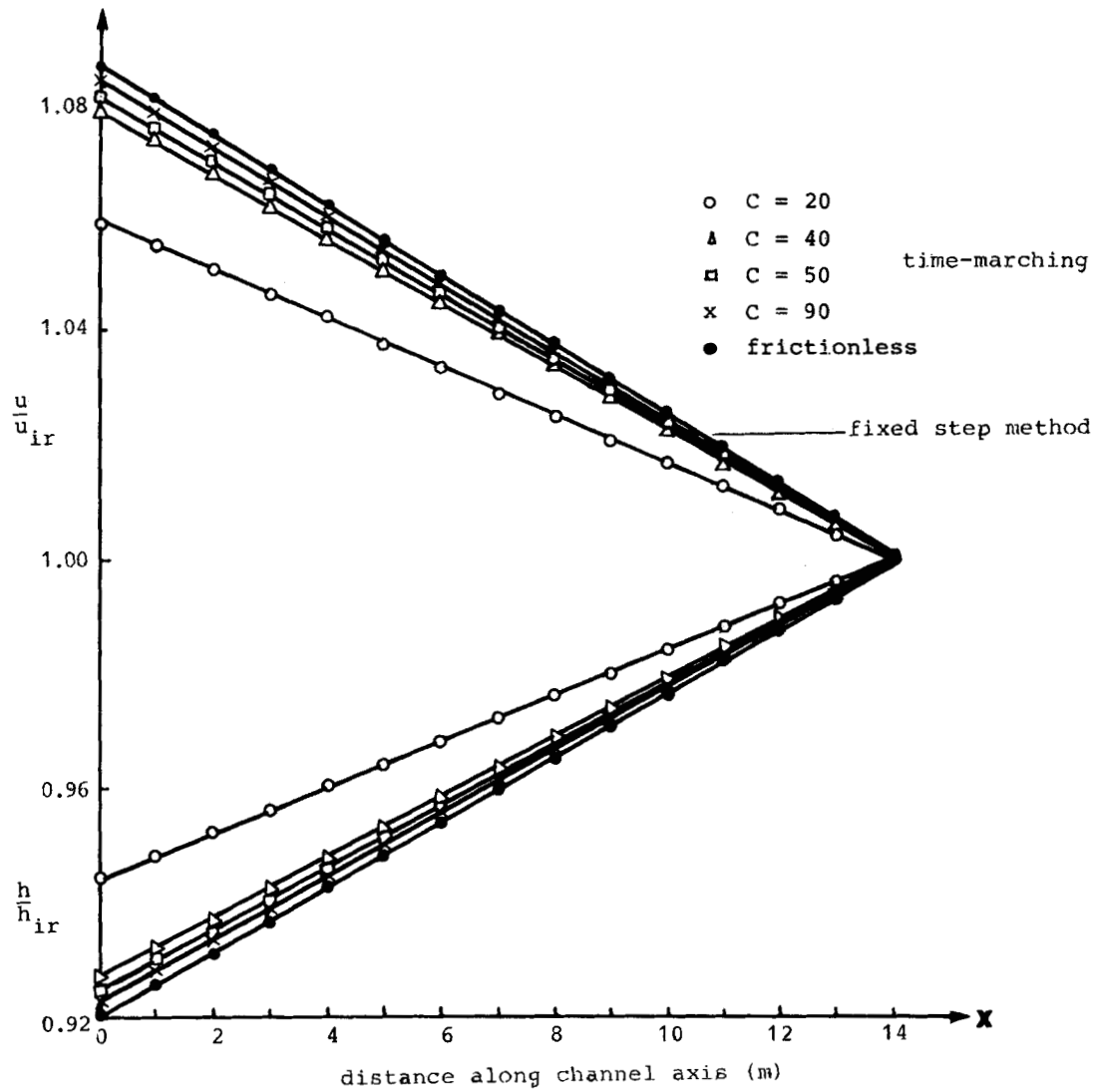

Figure 8. Comparison between time-marching and fixed step method predictions of subcritical velocity and depth distributions for straight parallel wall channel geometry at $Q = 20{\cdot}0\ \mathrm{m^3\ s^{-1}}$, $h_2 = 2{\cdot}0$ m and $S_{0x} = 0{\cdot}01$ using various Chézy friction coefficients

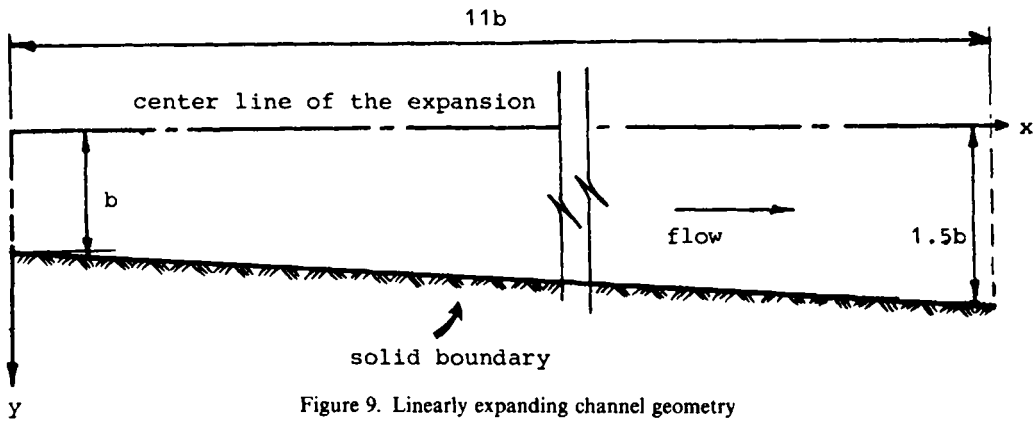

Figure 9. Linearly expanding channel geometry

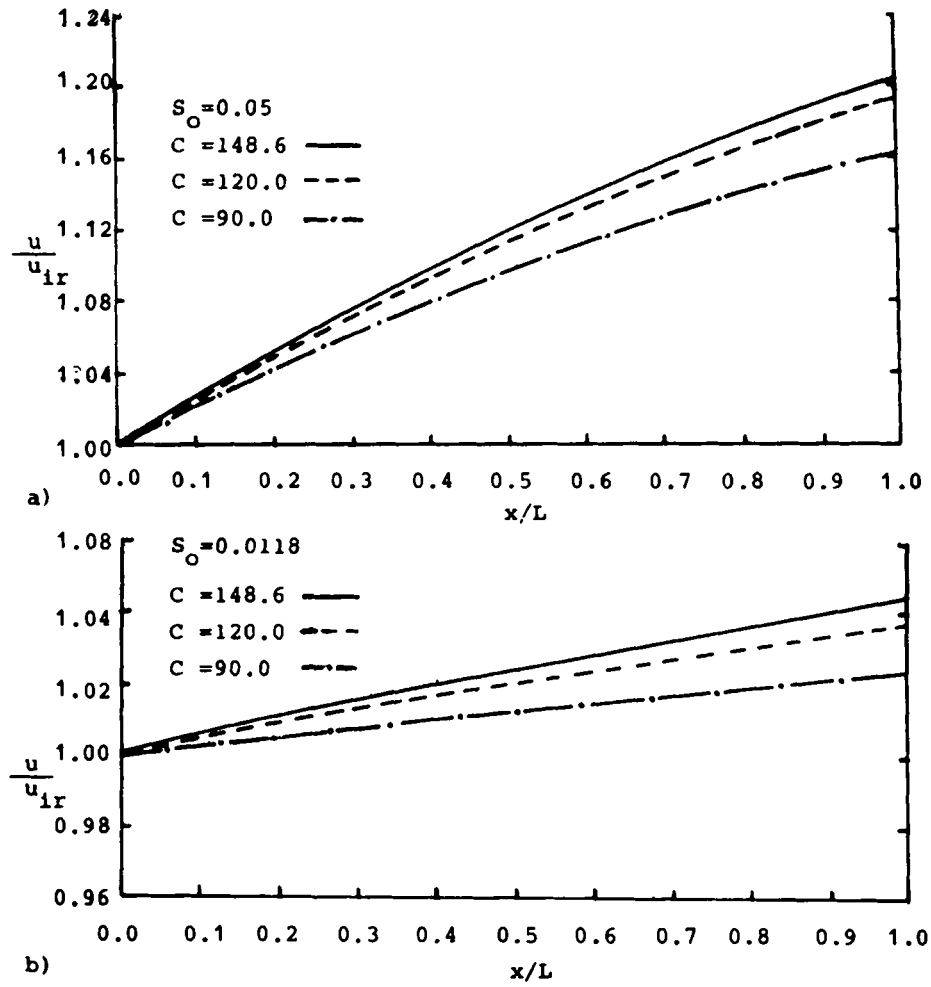

Figure 10. (a, b)

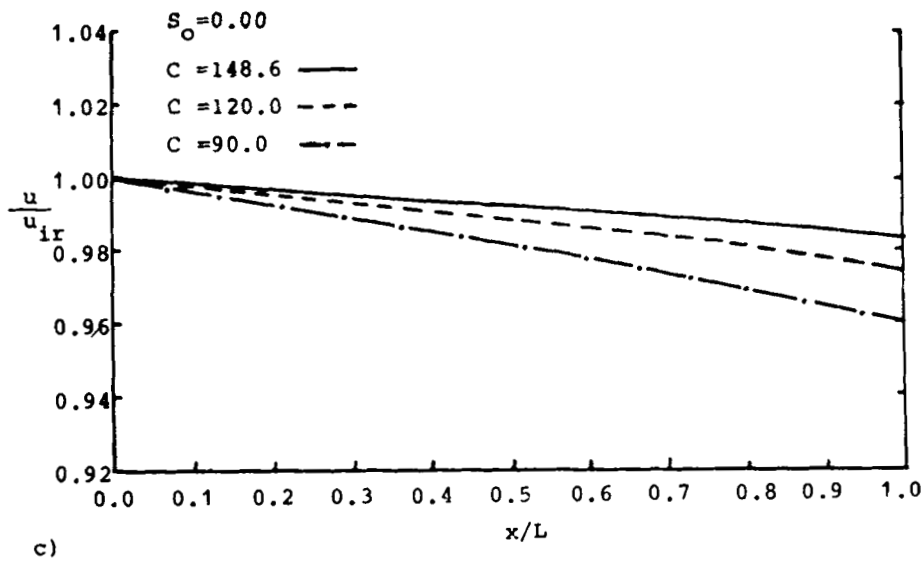

Figure 10. Time-marching predictions of the centreline velocity distributions for the linearly expanding channel at $Fr_1 = 2{\cdot}0$ using various slopes and Chézy friction coefficients

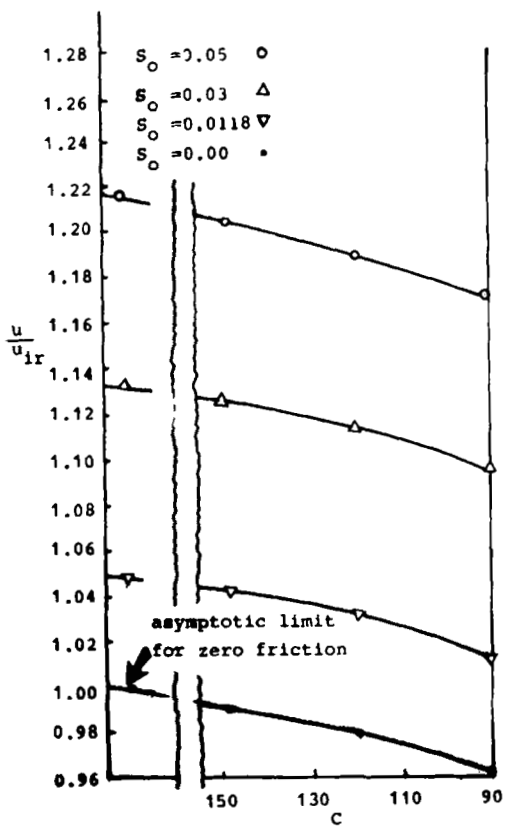

Figure 11. Time-marching predictions of exit velocity variation with channel slope for the linearly expanding channel at $Fr_1 = 2{\cdot}0$, $h/b = 0{\cdot}5$ and $v_1 = 0\ \mathrm{m\,s^{-1}}$ using various Chézy friction coefficients

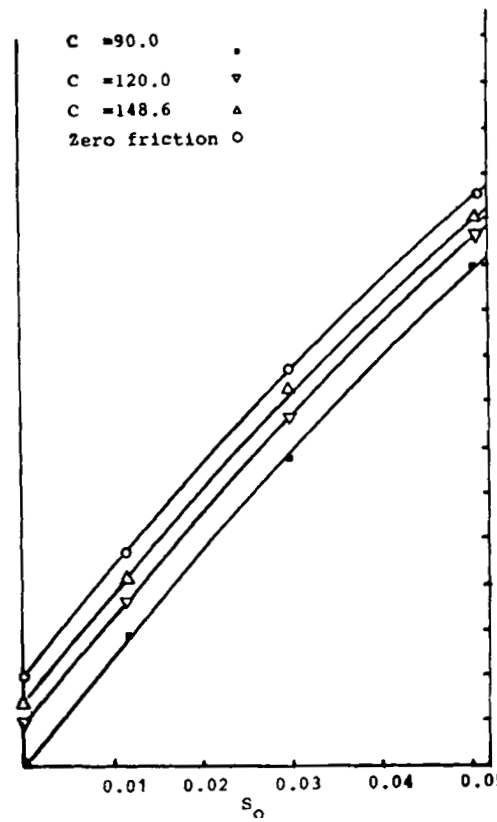

Figure 12. Time-marching predictions of exit velocity variation with Chézy's friction coefficient for the linearly expanding channel at $Fr_1 = 2{\cdot}0$, $h/b = 0{\cdot}5$ and $v_1 = 0\ \mathrm{m\,s^{-1}}$ using various channel slopes

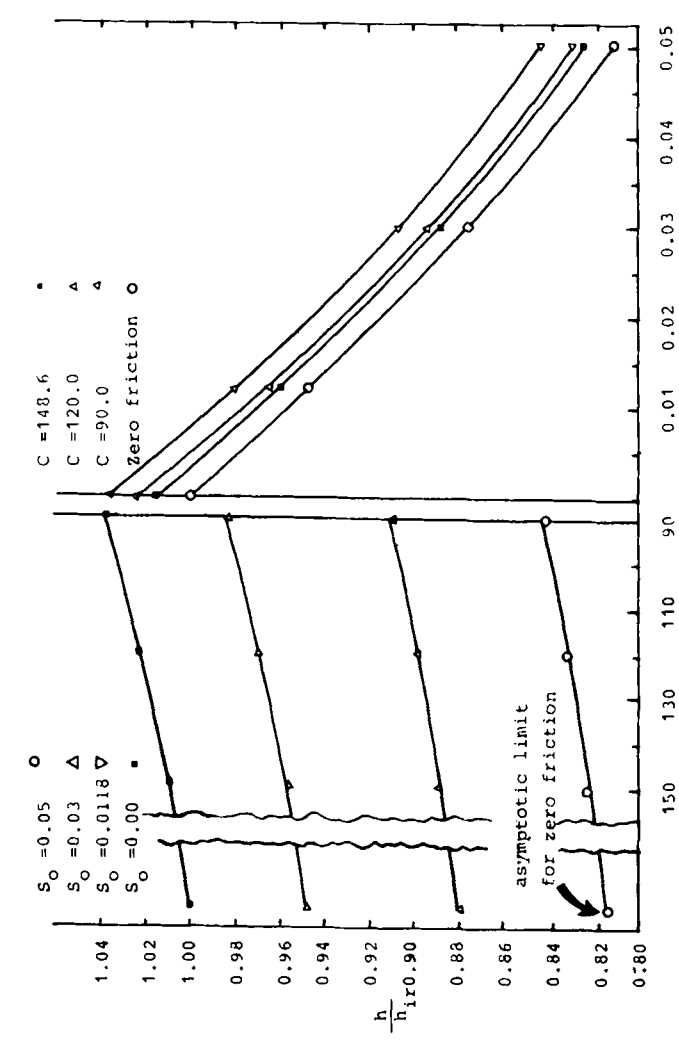

Figure 13. Time-marching predictions of exit depth variation with Chézy's friction coefficient for the linearly expanding channel at $Fr_1 = 2{\cdot}0$, $h/b = 0{\cdot}5$ and $v_1 = 0\ \mathrm{m\,s^{-1}}$ using various channel slopes

Figure 14. Time-marching predictions of exit depth variation with channel slope for the linearly expanding channel at $Fr_1 = 2{\cdot}0$, $h/b = 0{\cdot}5$ and $v_1 = 0\ \mathrm{m\,s^{-1}}$ using various Chézy friction coefficients

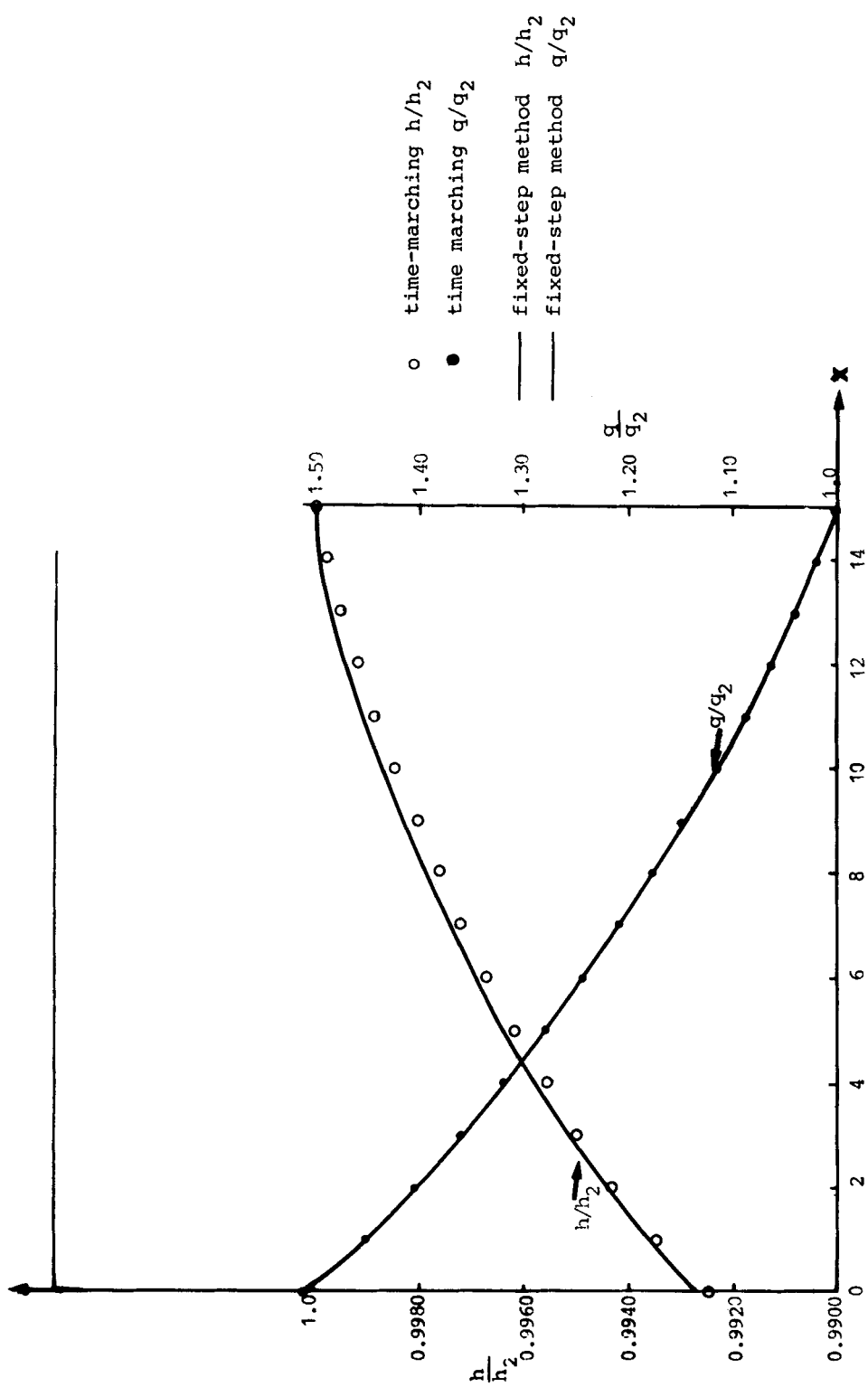

Figure 15. Comparison between time-marching and fixed step method predictions of subcritical velocity and depth distributions for linearly expanding channel ($L = 15{\cdot}0$ m)

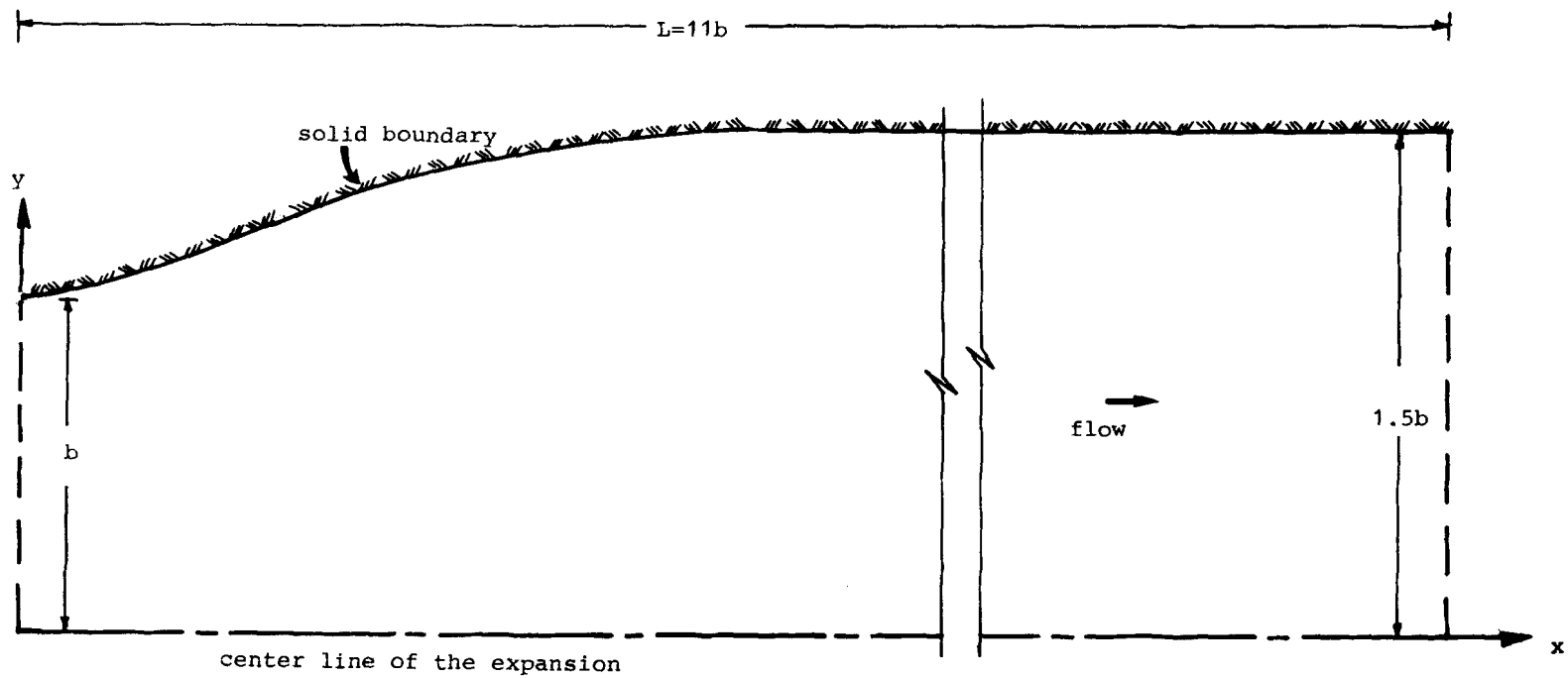

Figure 16. Design channel geometry after Rouse *et al.*[2]

designed using roughly the method of Rouse *et al.*[2] Their general design method was simplified[5] by using a Prandtl–Meyer table of the expansion functions which were generated by Liggett and presented in the thesis by Vasudev[13]. The expansion was designed for an entrance Froude number of 2·0 and a depth-to-width ratio h/b at entrance of 0·5. The length of the expansion is $11b$ and the final width $1{\cdot}5b$. Figures 17–19 show the comparisons between time-marching and characteristics[5] predictions of the centreline velocity distributions in the improved solution as compared to the frictionless zero-slope solution for various Chézy friction coefficients. For high values of C (Figures 17 and 18) the agreement is satisfactory. The agreement worsens at about 75%–100% of

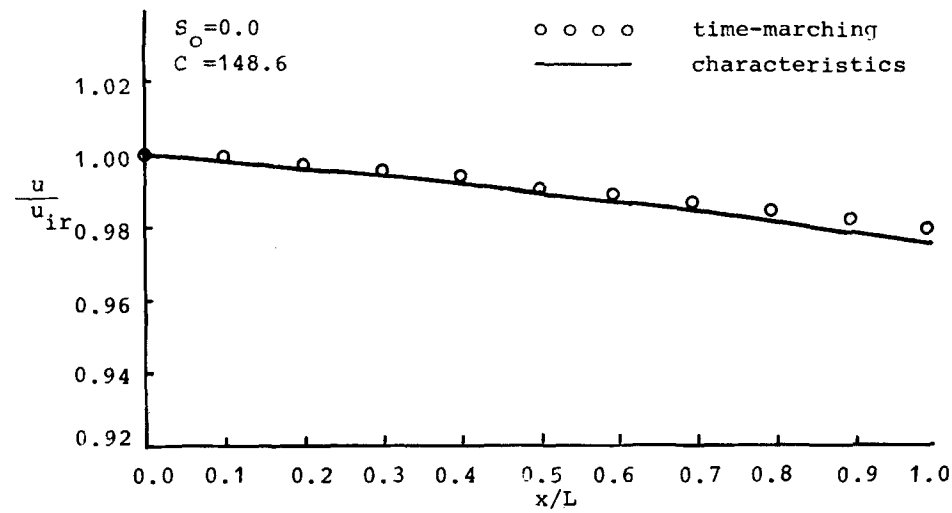

Figure 17. Comparison between time-marching and characteristics predictions of centreline velocity distributions for Rouse *et al.* channel at $Fr_1 = 2{\cdot}0$

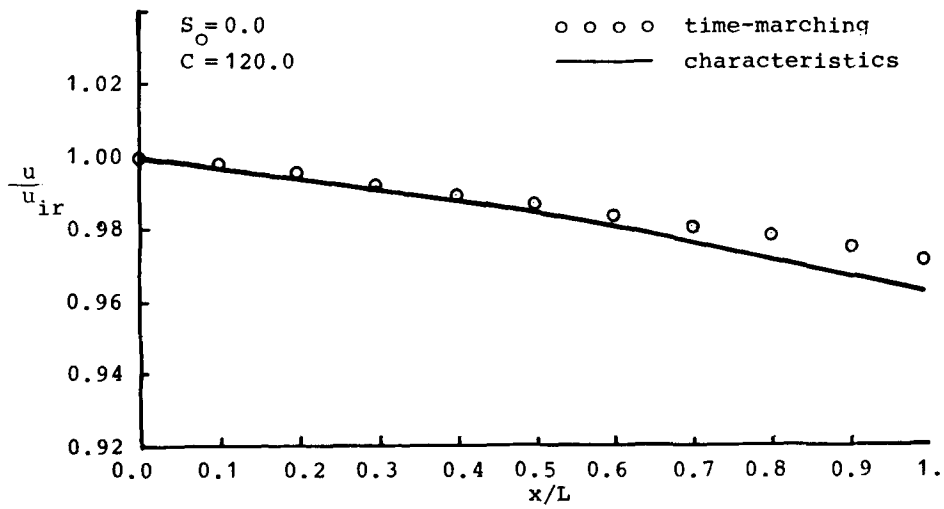

Figure 18. Comparison between time-marching and characteristics predictions of centreline velocity distributions for Rouse *et al.* channel at $Fr_1 = 2{\cdot}0$

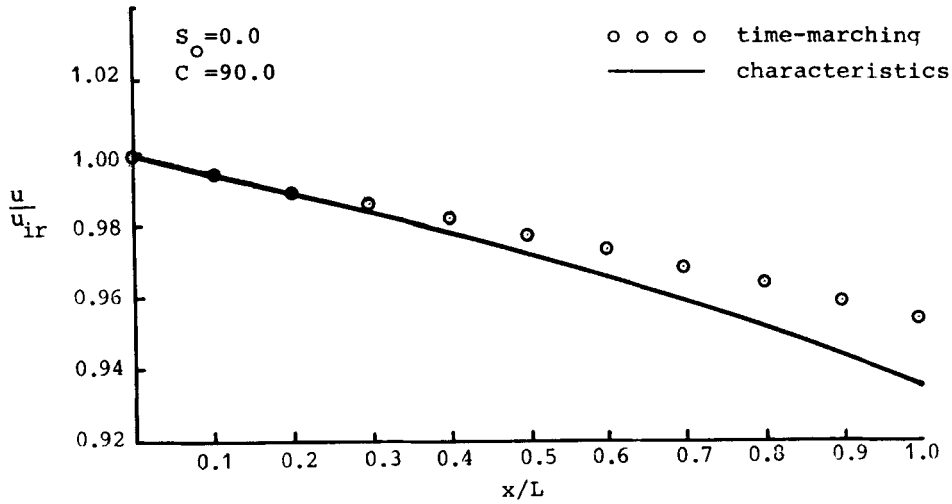

Figure 19. Comparison between time-marching and characteristics predictions of centreline velocity distributions for Rouse *et al.* channel at $Fr_1 = 2{\cdot}0$

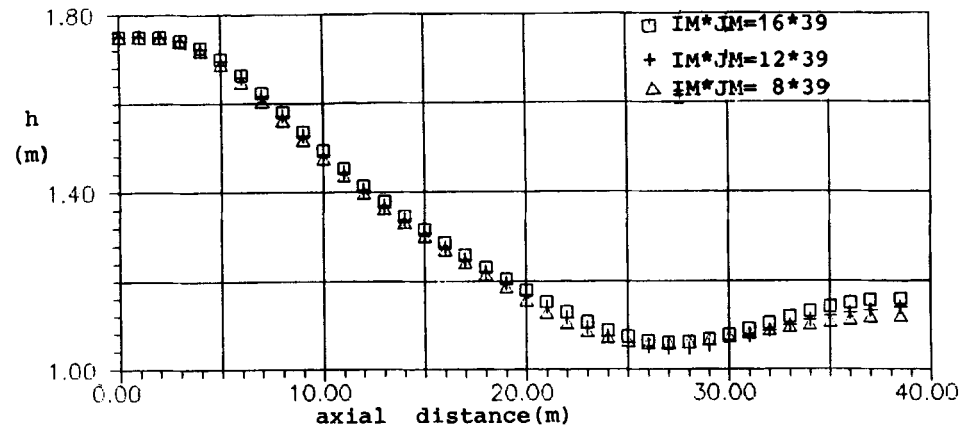

Figure 20. Predicted centreline water depth distributions for Rouse *et al.* channel at $Fr_1 = 2{\cdot}0$, $S_0 = 0{\cdot}0$ and $C = 90{\cdot}0$ using various $\Delta x{:}\Delta y$ ratios

x/L (Figure 19) where the friction is high. The computational grid was formed by finite volumes of $\Delta x{:}\Delta y \simeq 1{:}1$. The current test modelling has been carried out with an 8×39 grid. Grid reduction tests have shown (Figure 20) that the $\Delta x{:}\Delta y$ ratio does not essentially alter (maximum errors of less than 2%) the flow quantities.

CONCLUSIONS

A time-marching method, which has found wide application in computing turbomachinery flows, has been developed and applied to open channel flow calculations. The main advantage of the

method is the ability to deal readily with subcritical and supercritical types of flow; other very important features of the method are its great simplicity and the physical understanding obtained from the solution procedure. The presented time-marching method solves the equations of two-dimensional high-speed channel flow while including the usually neglected terms of slope and friction. It has been applied to a variety of open channel configurations in order to validate its potentialities. Charts are presented for an expansion channel which give an indication of the magnitude of the departure of the improved solution from the frictionless zero-slope solution. Comparisons with a characteristics method as well as with numerical solutions show that this approach is comparatively accurate, reliable and fast. It would be a relatively simple extension to program the equations for mixed continuous–discontinuous flows. The method can be utilized to eliminate the most common cause of spillway failures, namely the improper design of steep chutes. Straight walls are economical and perform satisfactorily in some physical situations. However, such walls may cause unacceptable surface waves in the downstream channel. The remedy is to use gently curving sidewalls. But this is a delicate problem, and whenever high velocity encounters an improperly designed side wall, large dynamic phenomena are created. The current method can be easily extended to design these side walls in order to obtain the desired flow distribution.

REFERENCES

1. A. Ippen, 'Mechanics of supercritical flow', *Trans. ASCE*, **116,** 347–363 (1951).
2. H. Rouse, B. V. Bhoota and En-Yun Hsu, 'Design of channel expansions', *Trans. ASCE*, **116,** (1951).
3. A. Busemann, *Gasdynamik. Handbuch der Experimental Physik* Vol. IV, 1931.
4. A. Ippen and J. H. Dawson, 'Design of supercritical contractions', *Trans. ASCE*, **116,** p. 326, (1951).
5. J. A. Liggett and S. U. Vasudev, 'Slope and friction effects in two-dimensional, high speed channel flow', *International Association for Hydraulic Research, 11th Int. Cong.*, Leningrad, 1965.
6. J. J. McGuirk and W. Rodi, 'A depth-averaged mathematical model for the nearfield of side discharges into open channel flow, *J. Fluid Mech.*, **86,** 761–781 (1978).
7. R. S. Chapman and C. Y. Kuo, 'Application of high accuracy finite-difference technique to steady free surface flow problems', *Int. J. numer. methods fluids*, **3,** 583–590 (1983).
8. R. S. Chapman and C. Y. Kuo, 'Application of the two equation k–ε turbulence model to a two-dimensional, steady, free-surface flow problem with separation, *Int. j. numer. methods fluids*, **5,** 257–268 (1985).
9. A. O. Demuren, 'Numerical computation of supercritical and subcritical flows in open channels with varying cross-sections', *Finite-Elements in Water Resources, Proc. 4th Int. Conf.*, Hannover, pp. 4.13–4.23, June 1982.
10. A. O, Demuren, 'Prediction of steady surface layer flows', *Ph.D. Thesis*, University of London, 1979.
11. D. B. Spalding, 'A general computer program for two dimensional parabolic phenomena', *HMT Series 1*, Pergamon Press, 1978.
12. F. Villegas, 'Design of the Punchiná spillway', *Water Power and Dam Construction*, 32–34 (November 1976).
13. S. U. Vasudev, 'Numerical investigations of supercritical flow', *Thesis*, Cornell University, 1963.
14. J. B. Herbich and P. Walsh, 'Supercritical flow in rectangular expansions', *J. Hydraul. Res. Div. Proc. ASCE*, **100,** 553–568 (1972).
15. D. Riabouchinsky, 'Sur l'analogie hydraulique des mouvements d'un fluide compressible', *C.R. Acad. Sci. Paris*, **195,** 998 (1932).
16. J. D. Denton, 'A time marching method for two and three dimensional blade to blade flows', *ARC R&M 3775, 1975.*
17. J. D. Denton, 'An improved time-marching method for turbomachinery flow calculation', *ASME Paper 82-GT-239*, 1982.
18. J. D. Denton, 'Solution of the Euler equations for turbomachinery flows. Part I: Basic principles and two dimensional applications', *NATO Advanced Study Institute on Thermodynamics and Fluid Mechanics of Turbomachinery*, Izmir, 17–28 September 1984, pp. 2.2.1–2.2.29.
19. M. A. Leschiner and W. Rodi, 'Calculation of strongly curved open channel flow', *J. Hydraul. Div. ASCE*, **105,** 1297–1314 (1979).
20. J. Kuipers and C. B. Vreugdenhil, 'Calculation of two-dimensional horizontal flow', *Reports S 163-I*, Delft Hydraulics Laboratory, 1973.
21. G. H. Lean and T. J. Weare, 'Modeling two-dimensional circulating flows', *J. Hydraul. Div. ASCE*, **105,** 17–26 (1979).
22. T. Arts, 'On the consistency of four different control surfaces used for finite-area blade to blade flow calculations', *Int. j. numer. methods fluids*, **4,** 1083–1095 (1984).

23. A. K. Rastogi and W. Rodi, 'Two and three dimensional calculations of heat and mass in open channel flows', *J. Hydraul. Div. ASCE*, 397 (1978).
24. B. P. Leonard, M. A. Leshziner and J. McGuirk, 'Third order finite-difference method for steady two-dimensional convection', *Proc. Int. Conf. on Numerical Methods in Laminar and Turbulent Flow*, Swansea, July 1978, pp. 807–819.
25. U. K. Singh, 'Computation of transonic flows in blade cascades with shock and boundary-layer interaction', *GEC J. Sci. Technol.*, **47**, (1981).
26. R. T. Knapp, 'Design of channel curves for supercritical flow', *Trans. ASCE*, **116**, 296 (1949).
27. W. H. Hager, 'Modified venturi channels', *J. Irrigation Drainage Eng. ASCE*, **111**, Paper no. 19563 (1985).
28. F. M. Neilson, 'Convex chutes in converging supercritical flow', *U.S. Army Engineer Waterways Experiment Station, Miscellaneous Paper H-76-19*, September 1976.